Doi: https://doi.org/10.1016/j.bej.2019.107296

Accepted Manuscript

Title: Modelling the Osmotic Behaviour of Human Mesenchymal Stem Cells

Authors: Elisa Casula, Gabriele Traversari, Sarah Fadda, Oleksiy V. Klymenko, Cleo Kontoravdi, Alberto Cincotti

PII: S1369-703X(19)30232-3
DOI: https://doi.org/10.1016/j.bej.2019.107296
Article Number: 107296

Reference: BEJ 107296

To appear in: *Biochemical Engineering Journal*

Received date: 5 November 2018
Revised date: 30 May 2019
Accepted date: 8 July 2019

Please cite this article as: Casula E, Traversari G, Fadda S, Klymenko OV, Kontoravdi C, Cincotti A, Modelling the Osmotic Behaviour of Human Mesenchymal Stem Cells, *Biochemical Engineering Journal* (2019), https://doi.org/10.1016/j.bej.2019.107296

Modelling the Osmotic Behaviour of Human Mesenchymal Stem Cells

Elisa Casula[1], Gabriele Traversari[1], Sarah Fadda[2], Oleksiy V. Klymenko[3], Cleo Kontoravdi[2] and Alberto Cincotti[1,*]

(1)Dipartimento di Ingegneria Meccanica, Chimica e dei Materiali, Facoltà di Ingegneria e Architettura, Università degli Studi di Cagliari, Via Marengo 2, 09123,Cagliari, Italy

(2) Centre for Process Systems Engineering, Department of Chemical Engineering, Imperial College London,

South Kensington Campus, London, SW7 2AZ, United Kingdom

(3) Department of Chemical and Process Engineering, Faculty of Engineering and Physical Sciences, University of Surrey, Guildford, GU2 7XH, United Kingdom

* Author to whom correspondence should be addressed (email: alberto.cincotti@dimcm.unica.it)

May 2019

Graphical abstract

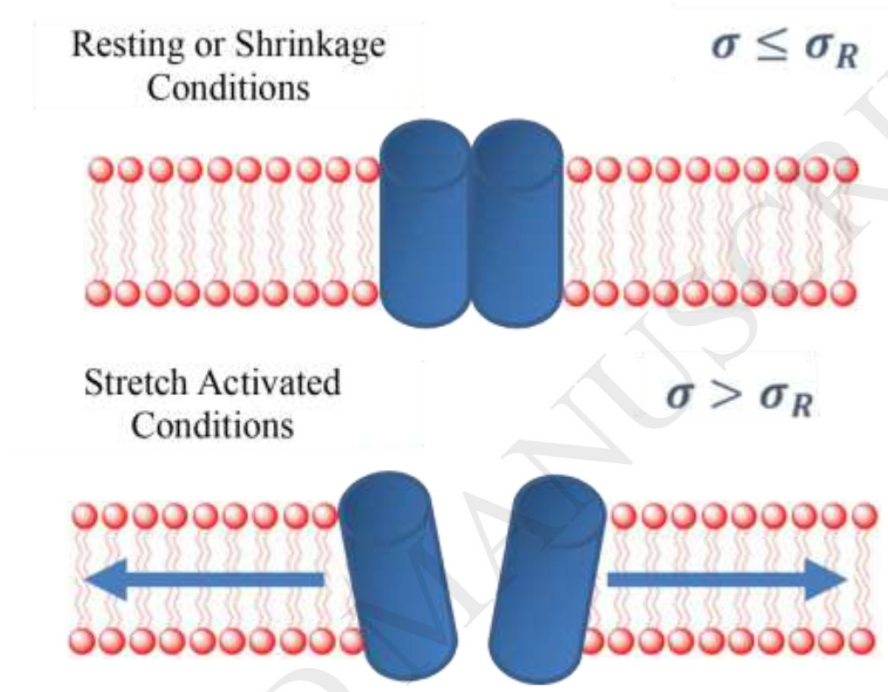

Highlights

- Non-perfect osmometer behavior of hMSCs from UCB described by a novel model.
- A coupling of cell osmosis with mechanics and SAR is considered.
- Mechanosensitive ion channels open when cell membrane stretches.
- Comparison with data provided: fitting and validation through prediction.

Abstract

In this work, a novel mathematical model for the description of the osmotic behavior during the cryopreservation of human Mesenchymal Stem Cells (hMSCs) from Umbilical Cord Blood (UCB) is proposed. In cryopreservation, the two-parameter formalism of perfect osmometer behavior is typically adopted and preferred due to its simplicity: cell volume osmotic excursions are described as due only to the passive trans-membrane transport of water and permeant solutes such as cryoprotectant agents (CPAs); intracellular solutes, responsible of the isotonic osmolality, are assumed to be impermeant. The application of the two-parameter model fails to capture the osmotic response of hMSCs whenever a swelling phase is involved, as demonstrated by the authors. To overcome this limitation, the imperfect osmometer behavior of hMSCs is successfully modelled herein by improving the two-parameter formalism through the coupling of osmosis with cell mechanics and cell membrane Surface Area Regulation (SAR): now the transmembrane permeation of solutes (ions/salt) during the swelling phase through the temporary opening of mechanosensitive channels is allowed. This way cells can reach an equilibrium volume different from the initial isotonic one, when isotonic conditions are re-established after contact with impermeant or permeant solutes, such as sucrose or dimethyl-sulfoxide (DMSO), respectively. The sequential best-fit procedure adopted to adjust model parameters is reported herein along with model validation through full predictions.

Keywords: hMSCs from UCB; Osmosis; Modelling; Mechanosensitive ion channels; Surface area regulation.

Notation

$E_{\mathrm{a,CPA}}$	activation energy for CPA permeation
$E_{\mathrm{a,Ions}}$	activation energy for ions/salt permeation
$E_{\mathrm{a,W}}$	activation energy for water permeation
h	membrane + cortex thickness
K	elastic modulus of cell membrane
k_{S}	rate of variation of reference surface of cell
L_{P}	water permeability
L_{P}^{∞}	pre-exponential factor for water permeation
M^{EXT}	extracellular osmolality
M^{INT}	intracellular osmolality
M^{I}	extracellular osmolality during phase I
M^{II}	extracellular osmolality during phase II

$M_{\mathrm{CPA}}^{\mathrm{EXT}}$	extracellular CPA osmolality
$M_{\mathrm{Ions}}^{\mathrm{EXT}}$	extracellular ions/salt osmolality
$M_{\mathrm{Sucrose}}^{\mathrm{EXT}}$	extracellular sucrose osmolality
$M_{\mathrm{CPA}}^{\mathrm{INT}}$	intracellular CPA osmolality
$M_{\mathrm{Ions}}^{\mathrm{INT}}$	intracellular ions/salt osmolality
$M_{\mathrm{Ions}}^{\mathrm{INT,0}}$	initial intracellular ions/salt osmolality
P_{CPA}	CPA permeability
P_{Ions}	Ions/salt permeability
$P_{\mathrm{CPA}}^{\infty}$	pre-exponential factor for CPA permeation
$P_{\mathrm{Ions}}^{\infty}$	pre-exponential factor for ions/salt permeation
r	cell radius
R	universal gas constant
S_{Ref}	reference area for cell membrane
S_{Sph}	cell membrane area
S_{Ref}^{0}	initial, reference area for cell membrane
S_{Sph}^{0}	initial, isotonic cell membrane area
t	Time
T	absolute temperature
V_{B}	inactive cell volume
V_{Cell}	cell volume
V_{CPA}	intracellular CPA volume
V_{Ions}	intracellular ions/salt volume
V_{W}	intracellular water volume
V_{Cell}^{0}	initial, isotonic cell volume
V_{W}^{0}	initial, isotonic intracellular water volume
V_{Ions}^{0}	initial, isotonic intracellular Ions/salt volume
V_{Cell}^{I}	cell volume at equilibrium after phase I
V_{Cell}^{II}	cell volume at equilibrium after phase II
V_{Ions}^{I}	ions/salt intracellular volume at equilibrium after phase I
V_{Ions}^{II}	ions/salt intracellular volume at equilibrium after phase II
$V_{\mathrm{Ions}}^{\mathrm{II,0}}$	ions/salt intracellular volume at the beginning of phase II
V_{W}^{I}	water intracellular volume at equilibrium after phase I
V_{W}^{II}	water intracellular volume at equilibrium after phase II
$V_{\mathrm{W}}^{\mathrm{II,0}}$	water intracellular volume at the beginning of phase II

ΔP	hydraulic pressure gradient
$\Delta\Pi$	osmotic pressure gradient
$\Delta\sigma$	variation of membrane tension
λ	adimensional parameter appearing in Equations 11-13, A8-A9
μ	adimensional parameter appearing in Equations 10-13, A6-A9
v_{B}	inactive cell volume fraction
$\tilde{v}_{\mathrm{CPA}}$	molar volume of CPA
$\tilde{v}_{\mathrm{Ions}}$	molar volume of ions/salt
Π^{EXT}	extracellular osmotic pressure
Π^{INT}	intracellular osmotic pressure
σ	membrane tension
σ_{R}	membrane resting tension
φ	dissociation constant for salt in water

1. Introduction

Human Mesenchymal Stem Cells (hMSCs) are considered a promising candidate for the regeneration and replacement of degenerated tissues [1]: adipogenic, chondrogenic and osteogenic differentiation is well acknowledged in the literature and has been investigated by many groups, as well as *in vitro* differentiation into cardiomyocytes, endothelial cells, and neuronal cells [2,3]. hMSCs are primarily collected by means of bone marrow aspiration, which is a painful and invasive procedure. For this reason, other sources such as Umbilical Cord Blood (UCB) need to be identified. Moreover, since proliferation and differentiation capabilities decrease with the age of donors [4], hMSCs from UCB show an improved proliferation and differentiation potential, and longer life span when compared to hMSCs from bone marrow of adults. On the other hand, isolation and collection of hMSCs from UCB has been reported to be difficult [4-7], and with uncertain results [8]. Thus, the preservation of these cells must guarantee the highest level of cell viability and functionality to enable effective tissue regeneration.

Currently, the most widely used method is cryopreservation which consists in maintaining cells at very low sub-zero temperatures (about -196 °C). The methodology involves several physico-chemical phenomena taking place during the osmotic equilibration with a cryo-protectant agent (CPA) and its removal, as well as the cooling and thawing phases: cell osmotic response to the contact with CPAs and their cytotoxicity, intracellular ice or glass formation and disappearance. These phenomena are strictly interrelated and depend on the working conditions. Physicochemical changes in cells often lead to a decrease in their viability and functionality [9-10]. In this context, the optimization of operating conditions is crucial. However, the number of experimental variables and parameters is too

large to permit any systematic exploration of experimental processing conditions. Rather, beneficial clues to best practices in cryopreservation can be obtained by numerical simulation [10], which allows the identification of most influential factors and a drastic reduction of experimental efforts provided the validity of the model can be ascertained in the range of conditions of interest.

Our recent experimental investigations of the osmotic behavior of hMSCs from UCB [6-7] revealed that these cells do not behave as perfect osmometers. Experimental findings indicate that positive cell volume excursions are limited during both the shrink-swell process following DMSO addition, and the restoration of isotonic conditions after the contact with hypertonic solutions of impermeant solutes (here called osmotic cycle with sucrose). On the other hand, when restoring the isotonic conditions following DMSO addition (here called osmotic cycle with DMSO), cell volume attains a final, equilibrium value that is different from the initial, isotonic one, depending on system temperature. Actually, this limited recovery of the initial isotonic volume of the cells varies not only with temperature but also with solutes concentrations and the number of osmotic cycles, since hysteretic phenomena were also observed.

In the field of cryopreservation, the two-parameter [11] or the Kedem and Katchalsky formalisms [12] are the two models typically adopted to interpret the osmotic behaviour of cells. They share the same basic assumption: the content of intra-cellular solutes responsible of the isotonic osmolality remains constant with time, since they are assumed to be impermeant through cell membrane (i.e. implying perfect osmometer behaviour). Water and permeant CPAs are merely described through passive diffusion transport mechanisms through cell membrane between ideal liquid solutions, albeit in the Kedem and Katchalsky formalism coupled diffusion is taken into account by the reflection coefficient, whereas it is independent in the two-parameter model. As a consequence, even though they differ in the dynamics followed to establish osmotic equilibrium between intra- and extracellular compartments, the two approaches share the same driving forces of material transport, and, consequently, the same equilibrium points. The locus of equilibrium cell volume is represented by the Boyle Van't Hoff plot. Accordingly, at isotonic conditions cells necessarily return to isotonic osmolality and to their original isotonic volume regardless of the osmotic path and volume excursion followed previously. It is worth noting that the two-parameter formalism is typically preferred to that of Kedem and Katchalsky due to its simplicity and the high selectivity of aquaporins, which exclude co-transport of water and CPA through the same channels [11].

Therefore, it is not surprising that iterative re-fitting of data is necessary to follow the osmotic response of hMSCs from UCB when the two-parameter model is adopted [6-7]. This means that estimates of model parameters vary depending on conditions while they are supposed to remain unchanged. This certainly greatly diminishes the model's predictive capability and the significance of inferred parameter values. This in turn leads to unrealistic model artefacts, most notably to an apparent increase of the inactive volume fraction (i.e. the volume of organelles, proteins and other

macromolecules that remains constant regardless of osmotic conditions; see below) depending on system temperature as well as solutes concentration, and number of osmotic cycles [6,7].

According to the biophysics and physiology literature, a much more complex picture than the one usually considered in cryopreservation studies with the two-parameter model emerges for the control of cell volume and shape [13-17]: in principle, the combined effect of mechanics (hydrostatics, active membrane contractility, membrane and cortical tension, cytoskeleton and its adhesion to membrane), electrical and chemical potentials (Gibbs-Donnan equilibrium, water and ion flows through passive and active channels) should all be taken into account to explain the osmotic response of a cell population, and the regulation of its surface area with membrane folds and blebs by means of exo- and endocytosis.

In particular, the pump-leak concept (i.e. an active influx of ions balanced, to preserve electro-neutrality, by a passive leak in the opposite direction) is well recognized as playing a role in the Regulatory Volume Decrease/Increase (RVD/I) following osmotic shocks, in combination with the folding/unfolding of cell membrane [13-16]. An increasing number of theoretical and experimental articles describe the cell SAR through variations of membrane tension and its relaxation mechanisms: microvilli and caveolae act as membrane reservoirs or sinks capable of quickly accommodating sudden mechanical stresses by exchanging part of the lipid bilayer with the main membrane in order to maintain tension homeostasis [18-23]. On the other hand, only a limited number of studies linking ion channels and cell osmotic regulation with cell mechanics are found in the literature [15,19].

Unfortunately, a quantitative understanding of the whole picture is still lacking, and a general model embedding all the phenomena described above is not yet available. On the other hand, a comprehensive mechanistic model may prove to be overparameterized, which may preclude its validation and a reliable determination of its parameter values. Moreover, when considered in the framework of the whole cryopreservation process, such a model would describe only the osmotic behavior of the cells while the cytotoxicity and ice/glass formation would still be left out. A further addition of these aspects to the model would likely render it intractable.

On the basis of these considerations, in this work the imperfect osmometer behavior of hMSCs is modelled and discussed as a conservative development of the two-parameter formalism: the idea is to minimize the increase in complexity compared with the widely adopted theoretical approach in cryopreservation to reasonably interpret the peculiar osmotic behavior of hMSCs. The novel model proposed here couples osmosis with cell mechanics and cell membrane SAR. The adopted fitting procedure is reported along with a validation of model's predictive power as well as an analysis of osmotic equilibrium conditions when contacting cells with impermeant solutes.

2. Model Equations

The failure of the two-parameter model to interpret the osmosis of hMSCs [6,7] prompted us to develop a new, improved model. In particular, the apparent increase in the inactive volume fraction needed to successfully fit the swelling phase of the osmotic cycle with impermeant sucrose using the two-parameter model, means that less cytosol (water and solutes) is exchanged with the environment to reach osmotic equilibrium at isotonic condition, resulting in a lower cell volume than the isotonic one. This lowering of exchangeable cytosol may be obtained only through its intra-cellular redistribution, by sequestration to form the so-called inactive (to osmosis) volume ($V_{\mathrm{Cytosol}} \rightarrow V_{\mathrm{B}}$), or extrusion to the surrounding environment ($V_{\mathrm{Cytosol}} \rightarrow \mathrm{Exterior}$). In the latter case, along with water, intra-cellular osmolytes, traditionally considered impermeant in the two-parameter model, can also exit the cell.

The first scenario was originally proposed in the 1930s for red blood cells by Ponder [24-26]. However, it seems unlikely that the inactive cell volume may increase by about 300%, according to the data measured by the authors for hMSCs [6-7], and it may be ruled out.

Conversely, the exchange of water and intra-cellular osmolytes is the basis of the pump-leak concept for ions. However, this approach involves active mechanisms such as ion pumps which consume energy. As such, they are considered only for long-term regulation of cell volume through RVD and RVI, but are typically neglected in cryopreservation, where only relatively short-term responses are taken into account. On the other hand, a passive diffusion mechanism coupling mechanics with osmosis recently appeared in the literature to model the exchange of ions/salt between intra- and extra-cellular compartments [15,17]. It was suggested that the presence of mechanosensitive (MS) ion channels triggered by osmotic excursions of cell volume may be responsible for the short-term response involved in cryopreservation. Expanding on this work, we propose an improvement to the two-parameter formalism by augmenting it with a model for SAR of the cellular membrane, describing the transient behavior due to osmosis and cell mechanics, thus mimicking homeostasis via endo- and exo-cytosis.

Dynamics

Referring to Figure 1, the typical salt-water sack model is adopted for a spherical cell, i.e., a volume of ideal, aqueous solution representing the cytoplasm is surrounded with a semipermeable phospholipid bilayer membrane, which regulates the exchange of water and solutes between the intra- and extracellular compartments. These exchanges may lead to variations in the total cell volume through changes in the volumes of intracellular water, V_{W}, and solutes, V_{Ions} and V_{CPA}:

$$V_{\mathrm{Cell}} = V_{\mathrm{B}} + V_{\mathrm{Ions}} + V_{\mathrm{W}} + V_{\mathrm{CPA}}. \quad (1)$$

A part of the total cell volume, V_{B}, corresponding to the nucleus, organelles, proteins, and other macromolecules, is supposed to be unaffected by the osmotic variations. The combined volume of organelles and macromolecules is denoted as $V_{\mathrm{B}} = \upsilon_{\mathrm{B}} V_{\mathrm{Cell}}^{0}$, where V_{Cell}^{0} is the initial isotonic cell

volume, and υ_B is the inactive volume fraction under isotonic conditions that remains constant and is considered a characteristic feature of the cell lineage.

In the model proposed herein, water exchange is determined by coupling osmosis with cell mechanics, so that a counter-gradient of hydrostatic pressure always opposes the osmotic pressure difference during any shrinkage as well as swelling phases [15,17]. Water exchange can then be described by passive diffusion or down-hill transport along the gradient of a combined potential $\Phi = P - \Pi$. Thus, the volume of water contained in a cell may vary with time according to the following equation and initial isotonic condition:

$$\frac{dV_W}{dt} = -L_P\, S_{Sph}(\Delta P - \Delta\Pi), \qquad V_W(0) = V_W^0 = V_{Cell}^0 - V_{Ions}^0 - V_B \qquad @ \quad t = 0, \tag{2}$$

where $\Delta P = P^{INT} - P^{EXT}$ is the hydrostatic driving force (see below), and $\Delta\Pi = \Pi^{INT} - \Pi^{EXT}$ is the classical osmotic driving force of the two-parameter model, with the osmotic pressure proportional to solutes concentration expressed in terms of osmolalities according to the Van't Hoff equation: $\Pi = RTM$ (all symbols are defined in the nomenclature section).

In particular, as external sucrose is considered to be impermeant, intra- and extra-cellular solutes osmolalities are determined as $M^{INT} = (M_{Ions}^{INT} + M_{CPA}^{INT})$ and $M^{EXT} = (M_{Ions}^{EXT} + M_{Sucrose}^{EXT} + M_{CPA}^{EXT})$ correspondingly. The components of M^{INT} are time-dependent, and are defined using molar volumes $\tilde{v}$, and dissociation constant φ for salt/ions ($M_{Ions}^{INT} = \frac{\varphi}{\tilde{v}_{Ions}}\frac{V_{Ions}}{V_W}$ and $M_{CPA}^{INT} = \frac{1}{\tilde{v}_{CPA}}\frac{V_{CPA}}{V_W}$). External osmolalities are assumed to be constant with time because the volume of the extracellular solution is significantly greater than the cumulative cytoplasm volume of the suspended cells ($\frac{V_{cells}}{V_{External}} \cong 10^{-4}$). According to Equation 2, the rate of water exchange is proportional to water permeability L_P, which follows an Arrhenius-type dependence on temperature $L_P = L_P^{\infty} exp\left(-\frac{E_{a,W}}{RT}\right)$, and to the varying surface area of the spherical cell volume $S_{Sph} = 4\pi\left(\frac{3V_{Cell}}{4\pi}\right)^{\frac{2}{3}}$.

The passive diffusion of permeant CPA through cell membrane surface area S_{Sph} is described by

$$\frac{dV_{CPA}}{dt} = \tilde{v}_{CPA}\, P_{CPA} S_{Sph}\left(M_{CPA}^{EXT} - M_{CPA}^{INT}\right), \qquad V_{CPA}(0) = V_{CPA}^0 \quad @ \quad t = 0, \tag{3}$$

where the same kind of temperature dependence is adopted for CPA permeability: $P_{CPA} = P_{CPA}^{\infty} exp\left(-\frac{E_{a,CPA}}{RT}\right)$.

With the exception of the hydrostatic driving force ΔP appearing in Equation 2, the two equations reported above represent the two-parameter formalism, with water osmosis driven by the gradient of total solutes osmolalities between the two facing compartments, whereas the independent permeation of CPA is caused only by the gradient of this solute. It is worth noting that, the very standard version of the two-parameter model is with S_{Sph} fixed to its initial value, even if it may be left free to vary as formerly noted by Kleinhans [11]. Moreover, the assumption of ideal, dilute solutions already made in the original two-parameter model by Kleinhans [11] could be removed by following the

thermodynamics approach developed by Elliott and co-workers [27,28]. But this is out of the scope of this paper, where a different deviation from the classic two-parameter model is proposed.

The instantaneous mechanical response ΔP to osmotic shock $\Delta \Pi$ is determined by in-plane tension of the cell membrane, schematically depicted in Figure 1 by red curved arrows. In particular, during swelling in hypotonic conditions, as water enters the cell, its membrane surface area must increase to accommodate the new volume. This growth is sustained by membrane reservoirs activated through a temporary increase of cell membrane tension. Thus, the stretching of the cell membrane produces a force pushing inward (see the straight red arrow pointing towards the center of the spherical cell in Figure 1). According to the Laplace's law, this increase in membrane tension, $\Delta\sigma$, is mechanically equilibrated by hydrostatic pressure so that:

$$\Delta P = P^{\mathrm{INT}} - P^{\mathrm{EXT}} = \frac{2\,h\,\Delta\sigma}{r}, \tag{4}$$

where h is the combined thickness of the membrane and cytoskeletal cortex, and r is the cell radius. Considering the cortex and the membrane as a single layer [15], h is assumed constant for simplicity, while the cell radius varies with time as $r = \left(\frac{3V_{\mathrm{Cell}}}{4\pi}\right)^{\frac{1}{3}}$.

During swelling, P^{INT} temporarily exceeds P^{EXT}, resulting in a net force pointing outward (see the straight blue arrow in Figure 1) which opposes the continuation of water influx by pushing water out of cell.

The variation of cell membrane tension is determined by the deviation of the actual tension σ from the resting tension σ_{R} of the cell membrane:

$$\Delta\sigma = \sigma - \sigma_{\mathrm{R}}. \tag{5}$$

Recent studies have established the key role of the membrane tension in the regulation of cell motility and morphology, but the mechanism of tension sensation and the precise relationship between the membrane tension and the cell mechanical properties are still unknown [29]. Different models have been proposed to describe the influence of tension on cell membrane surface area [18-21,23]. In this work, an elastic cortex model [15] is adopted to describe its mechanical behaviour, according to which:

$$\sigma = \frac{K}{2}\left(\frac{S_{\mathrm{Sph}}}{S_{\mathrm{Ref}}} - 1\right), \tag{6}$$

with K representing the elastic modulus of the cell membrane. Thus a linear stress-strain dependence is adopted, with strain being measured as deviation of S_{Sph} from a reference value S_{Ref}.

Under steady state conditions (regardless of whether this was preceded by a shrinkage or swelling in response to external stimuli), from a mechanical perspective, the cell is assumed to be in a resting state, characterized by the minimum surface-to-volume ratio corresponding to a spherical shape with the membrane surface area S_{Sph}, and a membrane resting tension $\sigma_{\mathrm{R}} > 0$. The latter quantity is regarded as a characteristic feature of a given cellular lineage. Under steady state conditions, according to Equation 5, $\Delta\sigma = 0$ so that the hydrostatic pressure difference in Equation 4 gives $\Delta P =$

0. This implies that the inward force shown in Figure 1 resulting from the membrane tension, in resting condition is mechanically equilibrated by the reaction of the cytoskeleton, while S_{Ref} in Equation 5 attains a specific value ($S_{\mathrm{Ref}} = S_{\mathrm{Sph}}\left(1+\frac{2\sigma_{\mathrm{R}}}{K}\right)^{-1}$). Thus, the reference value S_{Ref} for measuring the strain of the membrane is lower than S_{Sph}, as depicted in Figure 1: S_{Ref} represents the membrane surface area in a totally relaxed state (when $\sigma = 0$ and, correspondingly, $S_{\mathrm{Sph}} = S_{\mathrm{Ref}}$).

The variation of the plasma membrane tension affects also the cell SAR [30]. When the cell volume changes, the cell membrane responds by trying to recover homeostasis. The main hypothesis of SAR is that whenever the membrane tension increases, some extra lipid bilayer is recruited from accessible endomembrane reserves to recover the resting tension value. On the contrary, when the tension drops below its resting value the membrane becomes slack so that part of it needs to be removed into reserves to recover the resting tension (Figure 2). This way an equilibrium condition for surface area membrane can be always re-established. The nature of these reserves is not yet clear [31]. Minor increases in the membrane tension could be buffered by undulations of the membrane such as filopodia, microvilli, membrane ruffles [31,32] that flatten with increasing tension, while more dramatic tension increases involve the disassembly of caveolae [32]. Other mechanisms by which the membrane tension is maintained are blebs, when internal tension is higher than external one, and vacuole-like dilatations, in the opposite case. In addition to the readily available plasma membrane buffers, cells can modulate their membrane tension using endomembranes by exo- and endo-cytosis [32].

On the basis of these considerations, the temporal variation of the cell membrane reference surface area is assumed here to vary proportionally to the force ($S_{\mathrm{Ref}} \cdot \Delta\sigma$) exerted on it

$$\frac{dS_{\mathrm{Ref}}}{dt} = k_{\mathrm{S}}\,\Delta\sigma\,S_{\mathrm{Ref}}, \qquad S_{\mathrm{Ref}}(0) = S_{\mathrm{Ref}}^{0} = \frac{S_{\mathrm{Sph}}^{0}}{1+\frac{2\,\sigma_{\mathrm{R}}}{K}} \quad @ \quad t = 0, \tag{7}$$

with k_{S} representing a proportionality constant. The initial value of S_{Ref} corresponds to the resting conditions of initial isotonic cells. Alternatively, Equation 7 may be seen as the rate of membrane area generation, which is equivalent to the flux of lipid bilayer between the cell membrane and membrane reservoirs, and is proportional to the driving force $\Delta\sigma$.

Equations 6-7 represent the essential novelty of this work, allowing us to couple osmosis with SAR through cell mechanics, thus describing dynamic excursions of the cell membrane tension as being dependent on two different kinetics: a trigger by osmotic shocks, that is a rapid departure from resting tension the rate of which is proportional to water permeability L_{P}, followed by a relatively slow relaxation governed by k_{S}. Therefore, during swelling the momentary increase of the cell membrane tension can activate the opening of mechanosensitive ion channels distributed over the membrane surface area as depicted in Figure 3, while at resting condition or during shrinkage these channels remain closed [15]. Accordingly, ions/salt may permeate the cell membrane as per the following equation describing their passive diffusion through the cell membrane surface area S_{Sph}:

$$\frac{dV_{\mathrm{Ions}}}{dt} = P_{\mathrm{Ions}} S_{\mathrm{Sph}} \left(\mathrm{M}_{\mathrm{Ions}}^{\mathrm{EXT}} - \mathrm{M}_{\mathrm{Ions}}^{\mathrm{INT}} \right), \qquad V_{\mathrm{Ions}}(0) = V_{\mathrm{Ions}}^{0} = \frac{\left(V_{\mathrm{Cell}}^{0} - V_{\mathrm{B}}\right)}{1 + \frac{\varphi}{\tilde{v}_{\mathrm{Ions}} M_{\mathrm{Ions}}^{\mathrm{INT},0}}} \quad @ \quad t = 0, \tag{8}$$

where the independent permeation of salt/ions is governed only by the gradient of that solute (as it was for CPA in Equation 2), and the corresponding on/off permeability following an Arrhenius-type temperature dependence when the mechanosensitive channels are open and being zero when they are closed:

$$P_{\mathrm{Ions}} = \begin{cases} 0 & \sigma \le \sigma_{\mathrm{R}} \\ P_{\mathrm{Ions}}^{\infty} exp\left(- \frac{E_{\mathrm{a,Ions}}}{RT} \right) & \sigma > \sigma_{\mathrm{R}} \end{cases}. \tag{9}$$

The initial condition in Equation (8) deserves a comment. It is well-known that initial, isotonic intracellular osmolality is due not only to ions but also to other non-ionic solutes dispersed in the cytoplasm (and not accounted for by the inactive volume). However, in the proposed model the initial, intra-cellular isotonic osmolality is attributed to ions exclusively, so that its exchange is proportional to the gradient across cell membrane with the ions (PBS) dissolved in the external solution. Besides, if this assumption was removed, external ions could be exchanged based on the gradient of any extracellular solute like sucrose or CPA, as modelled for water in Equation 2. But this possibility is intentionally left out in the proposed model.

Equilibrium with impermeant solutes

The magnitude of the cell volume when osmotic equilibrium is reached can be determined by solving Equations 2-8 at steady state. To this aim, the analysis of proposed model benefits from making a distinction between the phases when cells are in contact with a solution containing or not the solute during an osmotic cycle with impermeant sucrose: first isotonic cells are contacted with hypertonic solutions of sucrose added to isotonic PBS until equilibrium is reached (this is called phase I, and cells shrink); then cells return to isotonic PBS until a new equilibrium point is reached (this is called phase II, and cells swell). This single osmotic cycle with impermeant sucrose corresponds to the experimental RUNS 1-3 (phase I) followed by RUNS 4-6 (phase II) whose operating conditions are detailed in Table 1. These experimental runs were performed by the authors [6,7]. The case of two consecutive osmotic cycles with impermeant sucrose corresponds to the experimental RUN 15 reported in Table 1 as well.

For the case of isotonic cells in contact with a hypertonic solution of sucrose (phase I), the classic Boyle Van't Hoff equation

$$\frac{V_{\mathrm{Cell}}^{\mathrm{I}}}{V_{\mathrm{Cell}}^{0}} = v_{\mathrm{B}} + \frac{(1 - v_{\mathrm{B}})}{1 + \mu} \left(\frac{M^{0}}{M^{\mathrm{I}}} + \mu \right), \tag{10}$$

ensuing from the two-parameter model is derived also from the proposed model, since no ion exchange takes place during shrinkage when membrane tension is always lower than the resting value and MS channels remain closed. In Equation 10, isotonic osmolality is reported as $M^{0} = M_{\mathrm{Ions}}^{\mathrm{INT},0}$, while the osmolality of the external hypertonic solution is represented by $M^{\mathrm{I}} = M^{\mathrm{EXT,\,I}} = M_{\mathrm{Ions}}^{\mathrm{EXT,I}} +$

$M^{\mathrm{EXT,I}}_{\mathrm{Sucrose}}$. For the sake of completeness, in Equation 10 the contribution of solutes to the initial cell volume at isotonic condition is taken into account by the term $\mu \cdot \frac{(1-\upsilon_{\mathrm{B}})}{1+\mu}$. Here $\mu = \frac{\tilde{\upsilon}_{\mathrm{Ions}}\, M^0}{\varphi}$ represents the ration between ions and water intracellular volumes at isotonic conditions: it is a very small number which could be safely neglected. The first term in Equation 10 is clearly the contribution of the inactive volume, while the term $\frac{(1-\upsilon_{\mathrm{B}})}{1+\mu} \cdot \frac{M^0}{M^{\mathrm{I}}}$ represents the contribution of the intracellular water.

A linear dependence between the cell volume at equilibrium and the inverse of the external osmolality allows the inactive volume fraction, υ_B, to be determined through a simple linear regression. It is worth noting that, the Boyle Van't Hoff equation (as derived from the two-parameter model at steady state) does not depend on temperature, and predicts a perfect osmometer behavior with $\frac{V^{\mathrm{I}}_{Cell}}{V^0_{\mathrm{Cell}}} = 1$ when isotonic condition $\frac{M^0}{M^{\mathrm{II}}} = 1$ are re-established (phase II of the osmotic cycle with sucrose, where $M^{\mathrm{II}} = M^{\mathrm{EXT,II}} = M^{\mathrm{EXT,II}}_{\mathrm{Ions}}$).

In the new model, on the other hand, the swelling in phase II causes the membrane to stretch and reach tensions above σ_{R} which leads to MS channels opening and causing a leakage of ions from the cells. Assuming that the relaxation time of membrane tension is larger than the characteristic time of ion and water permeations (i.e. k_{S} low, with L_{P} and P_{Ions} high) and ΔP is negligible with respect to $\Delta\pi$ in Equation 2, at osmotic equilibrium the following equation holds:

$$\frac{V^{\mathrm{II}}_{\mathrm{Cell}}}{V^0_{\mathrm{Cell}}} = \upsilon_{\mathrm{B}} + \frac{(1-\upsilon_{\mathrm{B}})}{1+\mu}\left(\frac{M^0}{M^{\mathrm{II}}} + \mu\right)\left(\frac{\mu+\lambda\frac{M^0}{M^{\mathrm{I}}}}{\mu+\lambda\frac{M^0}{M^{\mathrm{II}}}}\right), \tag{11}$$

with $\lambda = \frac{P_{\mathrm{Ions}}}{R\,T\,L_{\mathrm{P}}}$. Derivation of Equation 11 is reported in the Appendix. The contributions of inactive, water and ionic volume fractions is readily recognized. In particular, the last bracketed term on the right hand side of Equation 11 represents the deviation from the Boyle Van't Hoff equation (compare with Equation 10). It clearly depends on λ, the ratio between ion and water permeabilities: when $\lambda = 0$, Equation 11 is equal to the Boyle Van't Hoff equation since no leakage of ions actually takes place, and the new model reduces to the two-parameter model at equilibrium; however, as λ increases, the linear profile of the cell volume vs the reciprocal of external osmolality is lost, and a progressively lower cell volume is reached. Moreover, the permeabilities of water and ions can change differently with temperature ($E_{\mathrm{a,W}} \neq E_{\mathrm{a,Ions}}$). As a consequence, Equation 11 predicts a partial recovery of the isotonic cell volume that depends on system temperature.

The single osmotic cycle with sucrose represented by Equations 10 and 11 for the shrinking (I) and swelling (II) phases respectively, can be generalized to a series of n (≥2) osmotic cycles to obtain

$$\frac{V^{\mathrm{I(n)}}_{\mathrm{Cell}}}{V^0_{\mathrm{Cell}}} = \upsilon_{\mathrm{B}} + \frac{(1-\upsilon_{\mathrm{B}})}{1+\mu}\left(\frac{M^0}{M^{\mathrm{I(n)}}} + \mu\right)\prod_{\mathrm{i=2}}^{\mathrm{n}} \alpha^{(\mathrm{i\text{-}1})}, \tag{12}$$

$$\frac{V^{\mathrm{II(n)}}_{\mathrm{Cell}}}{V^0_{\mathrm{Cell}}} = \upsilon_{\mathrm{B}} + \frac{(1-\upsilon_{\mathrm{B}})}{1+\mu}\left(\frac{M^0}{M^{\mathrm{II(n)}}} + \mu\right)\prod_{\mathrm{i=1}}^{\mathrm{n}} \alpha^{(\mathrm{i})}, \tag{13}$$

where $\alpha^{(\mathrm{i})} = \left(\frac{\mu + \lambda^{(\mathrm{i})} \frac{M^0}{M^{\mathrm{I}(\mathrm{i})}}}{\mu + \lambda^{(\mathrm{i})} \frac{M^0}{M^{\mathrm{II}(\mathrm{i})}}} \right)$ and $\lambda^{(\mathrm{i})} = \frac{P_{\mathrm{Ions}}\left(T^{(\mathrm{i})}\right)}{R\, T^{(\mathrm{i})}\, L_{\mathrm{P}}\left(T^{(\mathrm{i})}\right)}$. The contributions of the inactive, water and ion volume fractions is easily recognized as above, and the deviation from the Boyle Van't Hoff Equation 10 is conveniently grouped in the last product term on the right hand side. In particular, the shrinking phase I of the second cycle (represented by Equation 12 with n=2) is still characterized by a linear profile of equilibrium cell volume $\frac{V_{Cell}^{\mathrm{I}(2)}}{V_{\mathrm{Cell}}^{0}}$ vs the reciprocal of external osmolality $\frac{M^0}{M^{\mathrm{I}(2)}}$. Actually, this linearity is preserved for every shrinking phase I in a series of n osmotic cycles, while is never obtained for any swelling phase II.

3. Results and discussion

This section first addresses the fitting of experimental data to estimate the parameters of the model proposed to interpret the osmotic behavior shown by hMSCs from UCB. This was measured by the authors under equilibrium and transient conditions, when contacting the cells at different temperatures with hypertonic solutions of sucrose or DMSO added to isotonic PBS [6-7] and then returning them to isotonic conditions. The operating conditions of the dynamic runs used in this section are detailed in Table 1.

Then, model validation is performed by checking model capabilities to fully predict the system behavior in experimental runs not used for regression.

Finally, the equilibrium conditions with an impermeant solute predicted by the proposed model are analyzed and discussed to gain a deeper insight into the osmotic effect of temperature, external osmolality and number of cycles.

gPROMS ModelBuilder software v4.0 is used to solve numerically the model as well as to perform the regression analyses.

Regression analysis

The proposed model represented by Equations 1-8 contains several parameters (namely, the inactive volume fraction, rate constant of SAR, temperature dependent permeabilities of water, ions and CPA), whose values need to be determined through regression. To improve reliability, instead of adjusting all of the model parameters simultaneously, in this work a sequential best-fitting procedure is adopted. It follows a series of steps characterised by a progressive increase of model complexity: first, determine only v_{B} from equilibrium runs in hypertonic solutions with sucrose at different osmolalities, but at constant temperature; then, keeping v_{B} constant at the value just estimated, determine L_{P}, P_{Ions}, and k_{S} from the dynamic runs of the osmotic cycle with sucrose at constant osmolality, but at three different temperatures (see runs 1-6 in Table 1); finally, keeping all the previous parameters constant,

determine P_{CPA} from the dynamic runs of the osmotic cycle with DMSO at constant osmolality, but three different temperatures (i.e., runs 7-12 in Table 1).

The operating conditions of the equilibrium runs used in the first step for determining v_{B} are not reported here and may be found in [6]. Figure 4 shows the Boyle Van't Hoff plot obtained when contacting isotonic hMSCs with hypertonic solutions of sucrose. As pointed out in the modelling section, in this case the proposed model represented by Equation 10 reduces to the classical linear profile of the Boyle Van't Hoff plot. An acceptable correlation is obtained for the linear regression ($R^2 = 0.99$), and the inactive volume fraction v_{B} results equal to 0.2.

This value is reported in Table 2 along with all the other parameters. To reduce their number in the regression analysis some are taken from the literature. This is the case for the resting tension σ_{R}, membrane thickness h, and elastic modulus K, the values of which are not available for the specific cells under investigation but may be found for similar lineages. In particular, the resting tension reported in Table 2 is obtained from the value of $\sigma_{\mathrm{R}} \cdot h = 413$ pN/μm reported for fibroblasts by [21] and the membrane thickness $h = 0.5$ μm for generic eukaryotic cells is taken from [15]. The elastic modulus K shown in Table 2 is for hMSCs from bone marrow, as provided by [33]. Since the hypertonic solutions of sucrose and DMSO used for the experimental runs described in Table 1 are based on isotonic PBS, NaCl is the salt taken as representative of the ions exchanged between the intra- and extra-cellular compartments. Accordingly, the values of $\tilde{v}_{\mathrm{Ions}}$ and φ reported in Table 2 are the molar volume and dissociation constants of sodium chloride, respectively.

The comparison between model fitting and experimental data measured under transient conditions for the osmotic cycle with impermeant sucrose at three different system temperatures is reported in Figure 5. Here the cell volume normalized to its isotonic value ($V_{\mathrm{Cell}}^{0} \approx 1800\ \mu\mathrm{m}^3$) is shown as a function of time: the exposure of cells to the hypertonic solution invariably induces shrinkage followed by swelling when isotonic conditions are restored. The higher the temperature, the higher the rate of volume variation during both the shrinking and swelling phases. Therefore, the higher the temperature, the faster the new equilibrium volume is reached by the cells. However, although the new equilibrium condition is independent of the temperature in the shrinking phase, it varies for the swelling phase, at the end of the osmotic cycle. Moreover, only a partial recovery of the initial isotonic volume is attained in the swelling phase: the deviation from the initial isotonic volume is more pronounced at low temperatures and decreases when the temperature increases. The model reproduces well all of the features of the osmotic behavior experimentally observed for hMSCs, providing reliable estimates of the temperature-dependent water and ions permeabilities (L_{P} and P_{Ions}), and SAR constant rate (k_{S}) for this cell lineage, as reported in Table 2. The fidelity of the novel model is certainly more than acceptable if compared to the two-parameter model that would simulate a complete recovery of the initial isotonic volume regardless of the temperature. The values obtained for water permeability fall into the relatively broad range of values reported in the literature for

different cell lineages [7]. On the other hand, from Table 2 an ions permeability equal to $6.91 \cdot 10^{-6}$ mol s^{-1} m^{-2} can be calculated at 300 K and isotonic osmolality: this value is slightly higher than the range 10^{-7}-10^{-6} mol s^{-1} m^{-2} reported in the literature for Na^{+} [15]. Besides, from the value found for k_S shown in Table 2, a characteristic time of about 330 seconds may be derived for cell membrane SAR at 300 K and isotonic osmolality. This time for membrane relaxation is much longer than the characteristic times corresponding to ions and water permeation (44 and 0.02 s, respectively). Moreover, from the values adopted for σ_R and h reported in Table 2, a characteristic ΔP equal to 10^2 Pa may be calculated from Laplace Equation (4) at initial cell radius. This hydrostatic pressure difference is much lower than the characteristic osmotic pressure difference $\Delta\pi = RT\ \Delta M$ equal to 7.5×10^5 Pa calculated at 300 K and isotonic osmolality difference. These justify the assumption made when deriving Equations 10-13.

The comparison between model fitting and experimental data measured under transient conditions for the osmotic cycle with permeant DMSO at three different temperatures is reported in Figure 6. In this case, the temporal profile of the normalized cell volume is characterized by the classical shrink-swell dynamics observed during the exposure to a hypertonic solution, followed by a swell-shrink excursion when isotonic conditions are restored. This is well-known behavior due to the relatively high water permeability in comparison with DMSO. In this case also, the higher the temperature the higher the rate of volume variation, and the faster the new equilibrium condition is reached by the cells. However, unlike in the previous case shown in Figure 5, the new equilibrium condition always depends on the temperature during both the exposure to a hypertonic solution and after restoring isotonic conditions. The model reproduces well all the details of the osmotic behavior experimentally observed for hMSCs, providing reliable estimates for this cell lineage of the temperature-dependent DMSO permeability (P_{CPA}) reported in Table 2. The obtained values for CPA permeability fall into the relatively broad range of values reported in the literature for different cell lineages as discussed in [7]. As in the above case, the fidelity of the novel model is certainly more than acceptable if compared with the two-parameter model that predicts, regardless of the temperature, a volume excursion beyond the initial isotonic volume at the end of exposure to a hypertonic solution, and its complete recovery when isotonic conditions are restored [7,35-36]. It is worth noting that the deviation from the perfect osmometer behavior predicted by the two-parameter model is more pronounced at low temperatures and reduces when the temperature increases.

Model validation

Finally, the predictive capability of the proposed model is validated using test data from experimental runs performed under transient conditions when contacting cells with hypertonic solutions of DMSO of two different osmolalities but at constant temperature (see Figure 7), and data from two consecutive osmotic cycles with sucrose at constant osmolality and temperature (see Figure 8).

In particular, the predicted effect of changing the external osmolality in the shrink-swell dynamics during DMSO addition is shown in Figure 7: when the concentration of the permeant solute is increased, a lower and anticipated minimum is reached during the cell volume excursion, as expected, and eventually a lower osmotic equilibrium value is attained. The prediction is sufficiently accurate considering the precision of experimental data. This is particularly true for run 14 where the external osmolality of DMSO is closer to the one used for the regression analysis, as expected. Note that, with the two-parameter model reproducing a perfect osmometer behavior, an equilibrium volume larger than the initial isotonic one would result due to DMSO addition, and the higher the external osmolality the higher the equilibrium cell volume [35].

In addition, the proposed model is capable of predicting with acceptable accuracy the progressive decrease of the equilibrium cell volume after each osmotic cycle with sucrose, as shown in Figure 8. This is particularly true for the first cycle which resembles the operating conditions used during the regression analysis, as expected. However, the prediction may be considered acceptable even for the second cycle (model accuracy is within 6% even for the second cycle): in this case, the perfect osmometer behavior would predict a complete recovery of the initial, isotonic volume at the end of every cycle.

Equilibrium conditions with impermeant solute

The equilibrium conditions obtained from the proposed model for an osmotic cycle with impermeant sucrose are reported in Figure 9. Specifically, the black line corresponds to Equation 10 and it shows, for initially isotonic cells, the equilibrium volume in the shrinkage phase I as a function of the reciprocal external osmolality. It can be seen that increasing the external osmolality of sucrose leads to more extensive shrinkage of the cell volume regardless of the temperature, and the obtained linear profile is characteristic of the BVH plot. Thus, for an external sucrose osmolality of 300 $\frac{mOsm}{L}$ the equilibrium cell volume equal to 60% of the initial isotonic one is attained, independently of the system temperature. The temperature only affects the time required to reach the equilibrium point. Starting from this, the red, blue and purple curves correspond to Equation 11 and represent, at three different temperatures, the equilibrium volume during the following swelling phase II in the osmotic cycle with sucrose. For the sake of comparison, the three temperatures considered here and the sucrose osmolality of 300 $\frac{mOsm}{L}$ are exactly the same as those used for the experimental runs reported in Table 1 and Figure 5. Clearly, in the swelling phase II the temperature level affects not only the dynamics of the process, but also the final equilibrium point, which always results in a partial recovery of the initial isotonic volume when the isotonic osmolality is restored. This partial recovery is more pronounced at lower temperatures: the deviation of the proposed model from the perfect osmometer simulated by the two-parameter model increases at lower temperatures. To rationalize this system behavior, Figures 9b-9c show the water and ions volumic contributions corresponding to the

cell volume in Figure 9a. It is clear that during the shrinkage phase I of the osmotic cycle only intra-cellular water exits the cell, while the ion content remains constant at the initial, isotonic value. In this case, the proposed model reduces to the two-parameter model since during shrinkage the membrane tension diminishes and mechanosensitive ion channels do not open. On the contrary, during the following swelling phase II, ions leak out of the cell since ion channels are now open because of an increased membrane tension. According to Table 2, the temperature dependences of ions and water permeabilities are different: the relatively higher activation energy for the permeation of water with respect to that for ions leads to a lower value of λ in Equation 11 as the temperature increases. Therefore, the progressive tendency of the proposed model towards the perfect osmometer behaviour (i.e. a complete recovery of the initial isotonic volume when restoring isotonic conditions) is due to the water permeability being proportionally higher than the permeability of ions as the temperature increases: equilibrium conditions are reached exclusively due to water, which permeates much faster in comparison with ions at higher temperatures.

Figure 10 shows the effect of the external osmolality at constant temperature on the equilibrium conditions for the osmotic cycle with impermeant sucrose in terms of cell volume (see Figure 10a) as well as the corresponding water and ions contributions (see Figures 10b-10c). In this case, Equations 10 and 11 for the shrinkage and the following swelling phases, respectively, are plotted by varying the concentration of sucrose in the hypertonic solution during the contact with cells, before restoring the isotonic conditions. Partial recovery is always obtained, with ions leaking out of the cells only during the swelling phase. This leakage is larger for higher values of the external osmolality of sucrose, and, correspondingly, the partial recovery of the initial isotonic cell volume is more pronounced. This time, λ does not change since the temperature is constant. Now water and ions permeate at a constant rate in the three cases examined, and their variation cannot be deemed responsible for this behaviour. This effect is due to a larger excursion of the cell volume when increased sucrose osmolality is adopted for the shrinkage phase of the osmotic cycle: the larger the shrinkage the larger the swelling excursion to recover isotonic conditions, and the larger the resulting leakage of intra-cellular ions.

Finally, Figure 11 shows the cell volume variations during the two consecutive cycles with sucrose at the operating conditions of run 15 in Table 1 (the corresponding temporal variation is reported in Figure 8). Figure 11 is the graphical representation of Equations 12-13. Starting from cells at isotonic conditions, the sequence of shrinkage and swelling phases during the two cycles is represented by the black and red lines, respectively. In particular, in this plot the shrinkage phases are represented by the straight black lines pointing towards the common intercept which corresponds to the inactive volume fraction v_B, while the swelling phases are represented by the red curves. The progressive decrease of the equilibrium cell volume after each osmotic cycle with sucrose is evident. It occurs due to continuous leakage of ions taking place during every swelling phase, when mechanosensitive channels open due to membrane stretching.

4. Conclusions and future work

In this work, a novel mathematical model capable of describing the peculiar osmotic behavior of human Mesenchymal Stem Cells from Umbilical Cord Blood is proposed for the optimization of the cryopreservation protocol. These cells show a non-perfect osmometer response to osmotic shocks, which cannot be described by the simple two-parameter formalism typically adopted in cryopreservation studies. The new model couples osmosis with cell mechanics and cell membrane surface area regulation which allows trans-membrane permeation of solutes during the swelling phase through temporary opening of mechanosensitive ion channels in the cell membrane. Thus, cells can reach an equilibrium volume different from the initial isotonic one, when isotonic conditions are re-established after contact with impermeant or permeant solutes. The model, trained through data fitting for parameter estimation and validated through prediction of a test set of experimental runs, shows acceptable agreement with measured data.

Further validations need to be addressed given that the model predicts an elastic expansion of the cell membrane surface area (up to 30%) larger than what is reported in the literature for different cell lineages. For comparison, membrane expansion by 2-4 % has been reported for protoplasts [30,37], while excessive elastic membrane expansion could lead to cell lysis and may therefore be unrealistic. The dependence of the rate of membrane area variation upon tension can be revised in the future when experimental evidence and relevant measurements become available. A relevant experiment would be to analyse the elastic response of this cell lineage through indentation or pulling tethers in order to check if the relatively large membrane area expansion is realistic, and estimate the values of more specific elastic parameters (i.e. elastic modulus and resting tension).

Moreover, the hypothesis of the coexistence of different sources of membrane reservoirs should be investigated. Indeed, a practically instantaneous release of more accessible membrane reservoirs, i.e. unfolding of the membrane, could be considered as an elastic expansion of the cell surface. On the contrary, the release from endomembranes is considerably more sluggish in its contribution to an increase in the cell surface area.

Finally, additional investigation should be performed to analyse the behaviour of mechanosensitive ion channels in this specific cell lineage. The minimum opening tension could be measured through patch clamp analysis and atomic force microscopy, and the variation of the amount of intracellular ionic solutes could be investigated by fluorescence analysis to validate the simplifications made in this work.

Appendix

For the derivation of Equation 11 related to the equilibrium condition of phase II during the osmotic cycle with impermeant sucrose, it is worth noting that if SAR is relatively faster than water and ion permeations (i.e. k_S high, with L_P and P_{Ions} low), during swelling S_{Ref} rapidly catches up with the increasing S_{Sph}, under a pseudo-stationary regime. As a consequence no $\Delta\sigma$ (or ΔP) develops, and the

MS channels remain closed like during the shrinkage of phase I. In such a case, the cells behave as perfect osmometers during both shrinkage and swelling phases: only water is exchanged, the proposed model reduces to the two-parameter model, and the linear BVH plot (cf. Equation 10) is valid for phase I as well as phase II.

On the other hand, if membrane relaxation is relatively slow (i.e. k_S low, with L_P and P_{Ions} high), during phase II cells swell and membrane tension temporarily increases above σ_R. Now, MS channels open, and ions are exchanged as well as water until steady state and equilibrium condition are eventually reached. However, since during the return to isotonic PBS $M_{Sucrose}^{EXT,II} = 0$, if ΔP in Equation 2 is assumed negligible (i.e. ΔP (or $\Delta\sigma$) $\approx 0 \ll \Delta\pi$), Equations 2, 8 share the same driving force represented by the ions concentration gradient across cell membrane. This way a simple, linear relationship between increasing V_W and decreasing V_{Ions} is obtained by dividing Equations 2 and 8:

$$\frac{dV_W}{dV_{Ions}} = -\frac{L_P R\,T}{P_{Ions}}. \tag{A1}$$

This equation is first integrated, at constant temperature, from the beginning to the final equilibrium condition of phase II to obtain

$$V_W^{II} - V_W^{II,0} = -\frac{L_P R\,T}{P_{Ions}}\left(V_{Ions}^{II} - V_{Ions}^{II,0}\right). \tag{A2}$$

Equation (A2) is combined with the following equilibrium condition of ions concentration gradient

$$M^{II} = \frac{n_{Ions}^{INT,II}}{V_W^{II}} = \frac{\varphi\, V_{Ions}^{II}}{\tilde{v}_{Ions}\, V_W^{II}}, \tag{A3}$$

to derive water and ions contributions to the cell volume at equilibrium condition of phase II as a function of water and ions contributions to the cell volume at the beginning of phase II:

$$V_W^{II} = \frac{V_W^{II,0} + \frac{L_P R\,T}{P_{Ions}} V_{Ions}^{II,0}}{1 + \frac{L_P R\,T}{P_{Ions}} \frac{\tilde{v}_{Ions}}{\varphi} M^{II}} \tag{A4}$$

and

$$V_{Ions}^{II} = M^{II}\,\frac{\tilde{v}_{Ions}}{\varphi} V_W^{II} = M^{II}\,\frac{\tilde{v}_{Ions}}{\varphi}\,\frac{V_W^{II,0} + \frac{L_P R\,T}{P_{Ions}} V_{Ions}^{II,0}}{1 + \frac{L_P R\,T}{P_{Ions}} \frac{\tilde{v}_{Ions}}{\varphi} M^{II}}. \tag{A5}$$

Since the beginning of phase II corresponds to the final, equilibrium condition of phase I given by Equation 10, Equations (A4) and (A5) may be written as

$$V_W^{II} = \frac{\left(\frac{1-v_B}{1+\mu}\right)\frac{M^0}{M^I} V_{Cell}^0 + \left(\frac{L_P R\,T}{P_{Ions}}\right)\left(\frac{1-v_B}{1+\mu}\right)\mu\, V_{Cell}^0}{1 + \left(\frac{L_P R\,T}{P_{Ions}}\right)\frac{\tilde{v}_{Ions}}{\varphi} M^{II}}, \tag{A6}$$

and

$$V_{Ions}^{II} = M^{II}\,\frac{\tilde{v}_{Ions}}{\varphi} V_W^{II} = M^{II}\,\frac{\tilde{v}_{Ions}}{\varphi}\,\frac{\left(\frac{1-v_B}{1+\mu}\right)\frac{M^0}{M^I} V_{Cell}^0 + \left(\frac{L_P R\,T}{P_{Ions}}\right)\left(\frac{1-v_B}{1+\mu}\right)\mu\, V_{Cell}^0}{1 + \left(\frac{L_P R\,T}{P_{Ions}}\right)\frac{\tilde{v}_{Ions}}{\varphi} M^{II}}. \tag{A7}$$

These latter Equations may be rearranged as it follows:

$$\frac{V_{\mathrm{W}}^{\mathrm{II}}}{V_{\mathrm{Cell}}^{0}}=\left(\frac{1-v_{\mathrm{B}}}{1+\mu}\right)\frac{\frac{M^{0}}{M^{\mathrm{I}}}+\left(\frac{L_{\mathrm{P}}RT}{P_{\mathrm{Ions}}}\right)\mu}{1+\left(\frac{L_{\mathrm{P}}RT}{P_{\mathrm{Ions}}}\right)\frac{\tilde{v}_{\mathrm{Ions}}}{\varphi}M^{\mathrm{II}}}=\left(\frac{1-v_{\mathrm{B}}}{1+\mu}\right)\frac{\frac{M^{0}}{M^{\mathrm{I}}}+\frac{\mu}{\lambda}}{1+\frac{1}{\lambda}\frac{\mu}{M^{0}}M^{\mathrm{II}}}=\left(\frac{1-v_{\mathrm{B}}}{1+\mu}\right)\frac{\lambda\frac{M^{0}}{M^{\mathrm{I}}}+\mu}{\lambda+\frac{\mu}{M^{0}}M^{\mathrm{II}}}=\left(\frac{1-v_{\mathrm{B}}}{1+\mu}\right)\frac{M^{0}}{M^{\mathrm{II}}}\frac{\lambda\frac{M^{0}}{M^{\mathrm{I}}}+\mu}{\lambda\frac{M^{0}}{M^{\mathrm{II}}}+\mu},\tag{A8}$$

and

$$\frac{V_{\mathrm{Ions}}^{\mathrm{II}}}{V_{\mathrm{Cell}}^{0}}=\ M^{\mathrm{II}}\ \frac{\tilde{v}_{\mathrm{Ions}}}{\varphi}V_{\mathrm{W}}^{\mathrm{II}}=M^{\mathrm{II}}\ \frac{\mu}{M^{0}}\left(\frac{1-v_{\mathrm{B}}}{1+\mu}\right)\frac{M^{0}}{M^{\mathrm{II}}}\frac{\lambda\frac{M^{0}}{M^{\mathrm{I}}}+\mu}{\lambda\frac{M^{0}}{M^{\mathrm{II}}}+\mu}=\mu\ \left(\frac{1-v_{\mathrm{B}}}{1+\mu}\right)\frac{\lambda\frac{M^{0}}{M^{\mathrm{I}}}+\mu}{\lambda\frac{M^{0}}{M^{\mathrm{II}}}+\mu}.\tag{A9}$$

Equation 11 is finally derived from the conservation of volumes represented by Equation 1 applied at the equilibrium condition of phase II, that is by adding the inactive volume fraction v_{B} to water and ions volume fractions given by Equations (A8)-(A9), respectively. Equations 12-13 may be derived following the same line of reasoning.

Acknowledgements

The Regione Autonoma della Sardegna (Italy) is gratefully acknowledged for funding this research (Progetto L.7/2007 RAS, Bando 2012, CUP F71J12000900002). This project has received also funding from the European Union's Horizon 2020 research and innovation programme under grant agreement No 734434 and No 698165. The funders had no role in study design, data collection and analysis, decision to publish, or preparation of the manuscript.

G.T. performed his activity in the framework of the International PhD in Innovation Sciences and Technologies at the Università degli Studi di Cagliari, Italy. S.F. is currently working as consultant at Process Systems Enteprise (PSE) in London, United Kingdom. E.C. is currently working for the Italian Minister of Education (MIUR) in Cagliari, Italy.

References

[1] A. Caplan, Why are MSCs therapeutic? New data: new insight. J. Pathol. 217 (2009) 318-324.

[2] Hass R., Kasper C, Böhm S, Jacobs R., Different populations and sources of human mesenchymal stem cells (MSC): a comparison of adult and neonatal tissue-derived MSC, Cell Commun. Signaling 9:12 (2011) 1-14.

[3] Dimarino A.M., Caplan A.I., Bonfield T.L., Mesenchymal stem cells in tissue repair, Front. Immunol. 4 (2013) 1-9

[4] K. Bieback, S. Kern, H. Klüter, H. Eichler, Critical parameters for the isolation of mesenchymal stem cells from umbilical cord blood, Stem Cells 22 (2004) 625-634.

[5] Wexler, S.A., Donaldson C, Denning-Kendall P, Rice C, Bradley B, Hows J.M., Adult bone marrow is a rich source of human mesenchymal 'stem' cells but umbilical cord and mobilized adult blood are not, Br. J. Haematol. 121 (2003) 368-374.

[6] E. Casula, Asuni G.P., Sogos V., Cincotti A., hMSCs from UCB: isolation, characterization and determination of osmotic properties for optimal cryopreservation, Chem. Eng. Trans. 43 (2015) 265-270.

[7] E. Casula, Asuni G.P., Sogos V., Fadda S., Delogu F., Cincotti A., 2017. Osmotic behaviour of human mesenchymal stem cells: Implications for cryopreservation, Plos One, 12, e0184180. https://doi.org/10.1371/journal.pone.0184180

[8] Parekkadan B., Sethu P., van Poll D., Yarmush M.L., Toner M., Osmotic selection of human mesenchymal stem/progenitor cells from umbilical cord blood, Tissue Eng. 13 (2007) 2465-2474.

[9] Mazur P., Leibo S.P., Chu E.H.Y., 2-factor hypothesis of freezing injury. Evidence from chinese-hamster tissue-culture cells, Exp. Cell Res. 71 (1972) 345-355.

[10] Karlsson J.O., Toner M., Long-term storage of tissues by cryopreservation: critical issues. Biomaterials 17 (1996) 243-256.

[11] Kleinhans F.W., Membrane permeability modeling: Kedem-Katchalsky vs a two-parameter formalism, Cryobiology 37 (1998) 271-289.

[12] Kedem O., Katchalsky A., A thermodynamic analysis of the permeability of biological membranes to non-electrolytes, Biochim. Biophys. Acta 27 (1958) 229-246.

[13] Lang F., Busch G.L., Ritter M, Völkl H., Waldegger S., Gulbins E, Häussinger D., Functional significance of cell volume regulatory mechanisms, Physiol. Rev. 78 (1998) 247-306.

[14] Hoffmann E.K., Lambert I.H., Pedersen S.F., Physiology of cell volume regulation in vertebrates, Physiol. Rev. 89 (2009) 193-277.

[15] Jiang H.Y., Sun S.X., Cellular pressure and volume regulation and implications for cell mechanics, Biophys. J. 105 (2013) 609-619.

[16] Sachs F., Sivaselvan M.V., Cell volume control in three dimensions: water movement without solute movement, J. Gen. Physiol. 145 (2015) 373-380.

[17] Tao J., Sun S.X., Active biochemical regulation of cell volume and a simple model of cell tension response, Biophys. J. 109 (2015) 1541-1550.

[18] Rauch C., Farge E., Endocytosis switch controlled by transmembrane osmotic response and phospolipid number asymmetry, Biophys. J. 78 (2000) 3036-3047.

[19] Morris C.E., Wang J.A., Markin V.S., The invagination of excess surface area by shrinking neurons, Biophys. J. 85 (2003) 223-235.

[20] Sens P., Turner M.S., Budded membrane microdomains as tension regulators, Phys. Rev. E 73 (2006) 031918-1-0319184.

[21] Tinevez J.Y., Schulze U., Salbreux G., Roensch J., Joanny J-F, Paluch E., Role of cortical tension in bleb growth, PNAS 106 (2009) 18581-18586.

[22] Sinha B., Koster D., Ruez R., Gonnord P., Bastiani M., Abankwa D., Stan R.V., Butler-Browne G., Vedie B., Johannes L., Morone N., Parton R.G., Raposo G., SensP., Lamaze C., Nassoy P., Cells respond to mechanical stress by rapid disassembly of caveolae, Cell 144 (2011) 402-413.

[23] Pietruch A., Bruckner B.R., Janshoff A., Membrane tension homeostasis of epithelial cells through surface area regulation in response to osmotic stress, Biochim. Biophys. Acta 1833 (2013) 712-732.
[24] Macleod J., Ponder E., The measurement of red cell volume: IV. Alterations in cell volume in hypotonic plasma, J. Physiol. 77 (1933) 181-188.
[25] Macleod J., Ponder E., Solvent water in the mammalian erythrocyte, J. Physiol. 86 (1936) 147-152.
[26] Ponder E., The measurement of red-cell volume. Conductivity measurements, J. Physiol. 85 (1935) 439-49.
[27] Prickett R.C., Elliott J.A.W., Hakda S., McGann L.E., A non-ideal replacement for the Boyle van't Hoff equation, Cryobiology 57 (2008) 130-136.
[28] Ross-Rodriguez L.U., Elliott J.A.W., McGann L.E., Non-ideal solution thermodynamics of cytoplasm, Biopreserv. Biobank. 10 (2012) 462-471.
[29] Diz-Munoz A., Fletcher D.A., Weiner O.D., Use the force: membrane tension as an organizer of cell shape and motility, Trends Cell Biol. 23 (2013) 47-53.
[30] Morris C.E., Homann U., Cell surface area regulation and membrane tension, J. Memb. Biol. 179 (2001) 79-102.
[31] Titushkin I., Cho M., Distinct membrane mechanical properties of human mesenchymal stem cells determined using laser optical tweezers, Biophys. J. 90 (2006) 2582-2591.
[32] Gauthier N.C., Masters T.A., Sheetz M.P., Mechanical feedback between membrane tension and dynamics, Trends Cell. Biol. 22 (2012) 527-35.
[33] Yourek G., Hussain M.A., Mao J.J., Cytoskeletal changes of mesenchymal stem cells during differentiation. Asaio J. 53 (2007) 219-228.
[34] R.H. Perry, D.W. Green, J.O. Maloney, Perry's chemical engineers' handbook. 6th ed. McGraw-Hill chemical engineering series, New York, 1984.
[35] Fadda S., Cincotti A., Cao G., Rationalizing the equilibration and cooling stages of cryopreservation: the effect of cell size distribution, Aiche J., 57 (2011) 1075-1095.
[36] Fadda S., Cincotti A., Cao G., The effect of cell size distribution during the cooling stage of cryopreservation without CPA, Aiche J. 56 (2010) 2173-2185.
[37] Wolfe J., Dowgert M.F., Steponkus P.L., Mechanical Study of the Deformation and Rupture of the Plasma-Membranes of Protoplasts during Osmotic Expansions, J. Memb. Biol. 93 (1986) 63-74.

Table 1. Experimental runs under transient conditions.

Initial Condition	*RUN*	$M^{EXT}_{Sucrose}$ $\left[\frac{mOsm}{L}\right]$	M^{EXT}_{CPA} $\left[\frac{mOsm}{L}\right]$	T [K]
Isotonic cells in contact with sucrose – phase I (3 temperatures)	1	300	0	290
	2	300	0	300
	3	300	0	310
Returning to isotonic conditions after contact with sucrose – phase II (3 temperatures)	4	0	0	290
	5	0	0	300
	6	0	0	310
Isotonic cells in contact with DMSO – phase I (3 temperatures)	7	0	1700	290
	8	0	1700	300
	9	0	1700	310
Returning to isotonic conditions after contact with DMSO - phase II (3 temperatures)	10	0	0	290
	11	0	0	300
	12	0	0	310
Isotonic cells in contact with DMSO – phase I (2 concentrations)	13	0	700	300
	14	0	1200	300
Isotonic cells in contact with sucrose, followed by restoring of isotonic conditions – phase I and phase II, repeated (2 cycles)	15	300	0	300
		0	0	300

Table 2. Model parameters

Parameter	Value	Unit	Reference
$E_{a,CPA}$	72570	[J mol^{-1}]	This work
$E_{a,Ions}$	22150	[J mol^{-1}]	This work
$E_{a,W}$	50000	[J mol^{-1}]	This work
h	0.5	[µm]	[15]
K	33000	[Pa]	[31]
k_S	$3.7 \cdot 10^{-6}$	[Pa^{-1} s^{-1}]	This work
L_P^{∞}	64.2	[µm Pa^{-1} s^{-1}]	This work
P_{CPA}^{∞}	$1.268 \cdot 10^{12}$	[µm s^{-1}]	This work
P_{Ions}^{∞}	$4.47 \cdot 10^{-3}$	[µm L s^{-1} mOsm^{-1}]	This work
R	8.314472	[J mol^{-1} K^{-1}]	[32]
σ_R	826	[Pa]	[15,21]
v_B	0.2	[-]	This work
$\tilde{v}_{CPA}$	$7.1 \cdot 10^{-5}$	[m^3 mol^{-1}]	[32]
$\tilde{v}_{Ions}$	$2.7 \cdot 10^{-5}$	[m^3 mol^{-1}]	[32]
φ	2	[-]	[33]

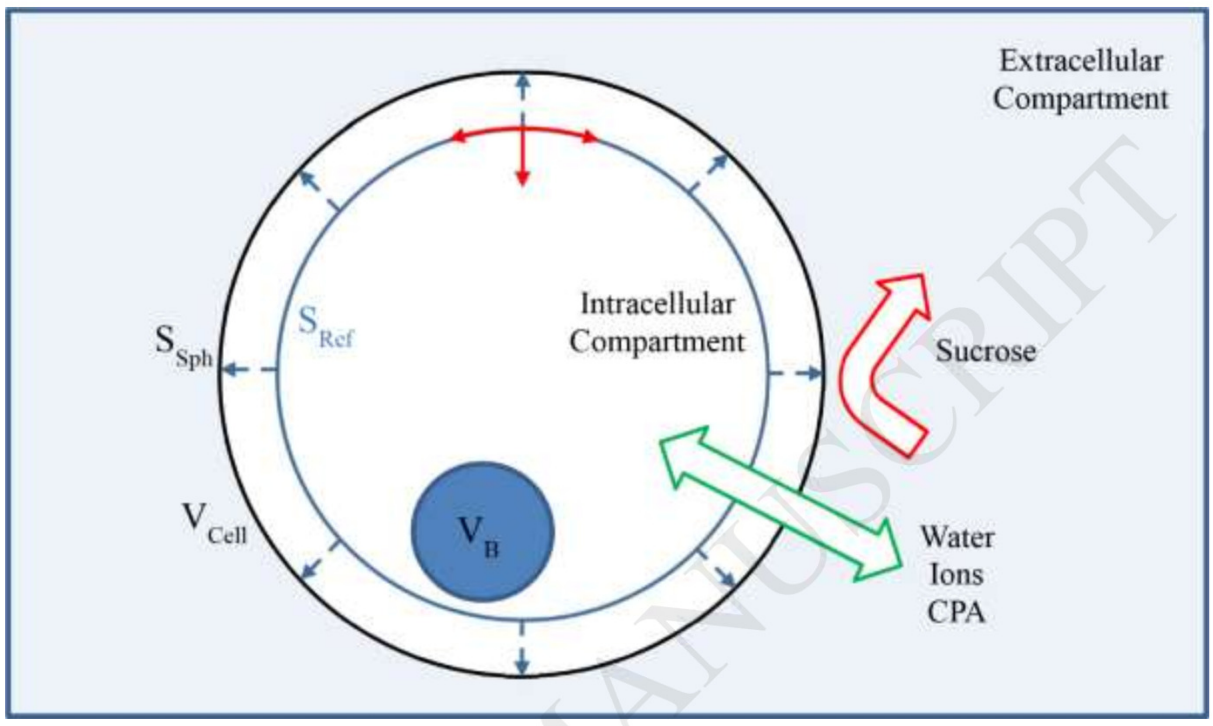

Figure 1: Schematic representation of a cell according to the “saltwater sack” model.

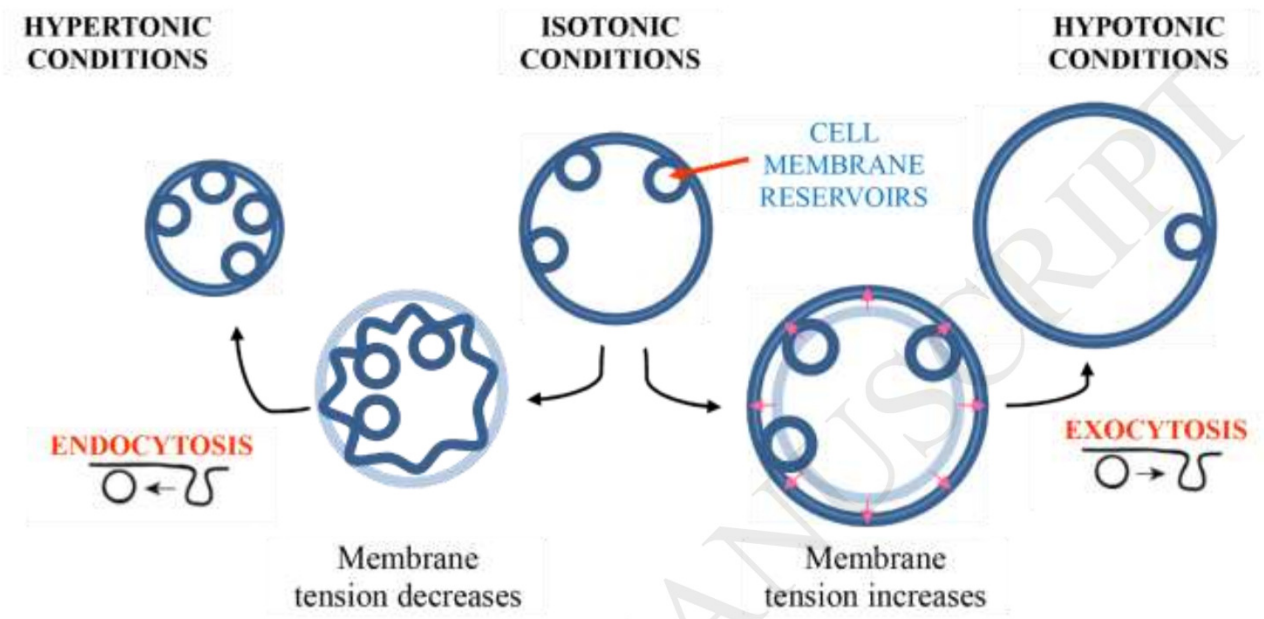

Figure 2: Schematic representation of cell membrane SAR: endocytosis under hypertonic conditions and exocytosis under hypotonic conditions.

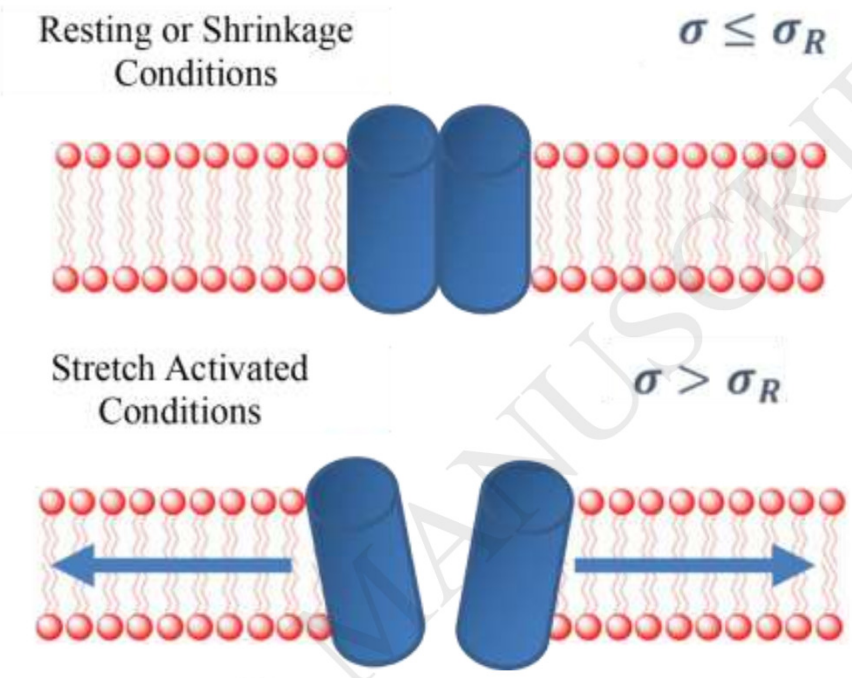

Figure 3: Schematic representation of activation mechanism for the mechanosensitive channels.

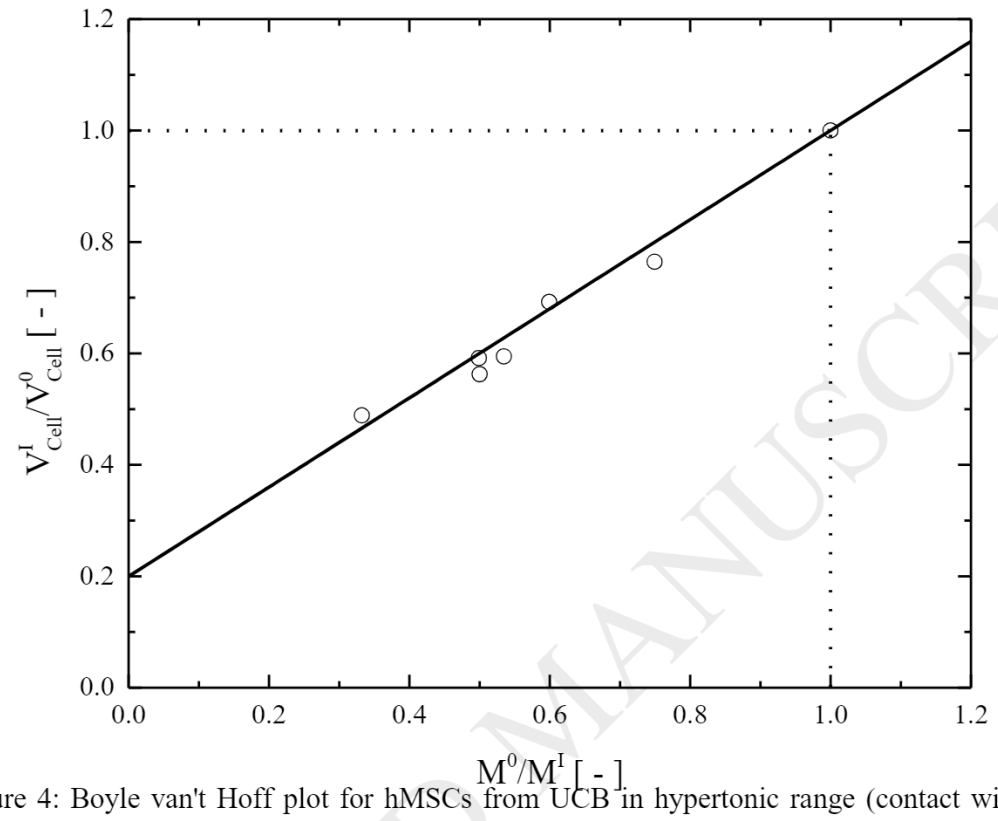

Figure 4: Boyle van't Hoff plot for hMSCs from UCB in hypertonic range (contact with sucrose at 300 K). $M^0 = M^{\mathrm{INT},0}_{\mathrm{Ions}}$, $M^I = M^{\mathrm{EXT,I}} = M^{\mathrm{EXT,I}}_{\mathrm{Ions}} + M^{\mathrm{EXT,I}}_{\mathrm{Sucrose}}$. Data measured by the authors [6].

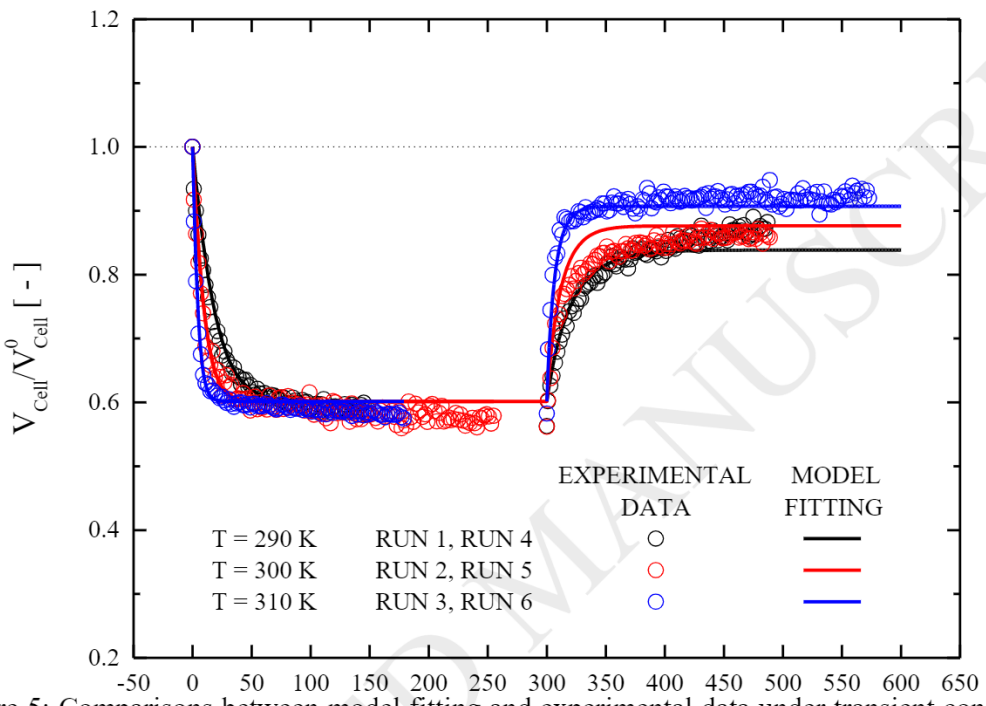

Figure 5: Comparisons between model fitting and experimental data under transient conditions for an osmotic cycle with sucrose. Data measured by the authors [6-7].

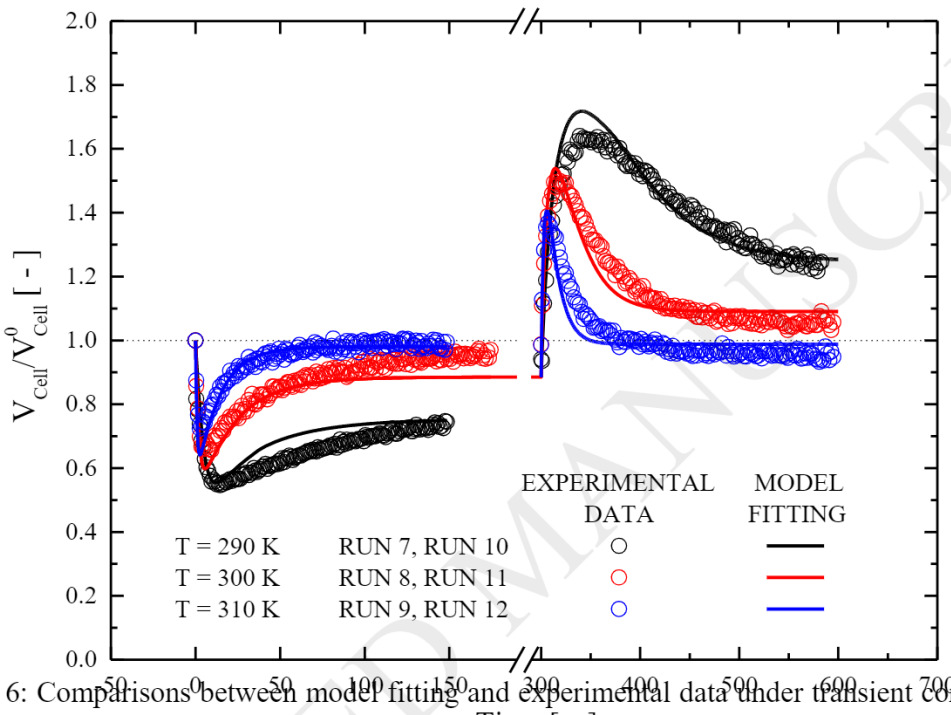

Figure 6: Comparisons between model fitting and experimental data under transient conditions for an osmotic cycle with DMSO. Data measured by the authors [6-7].

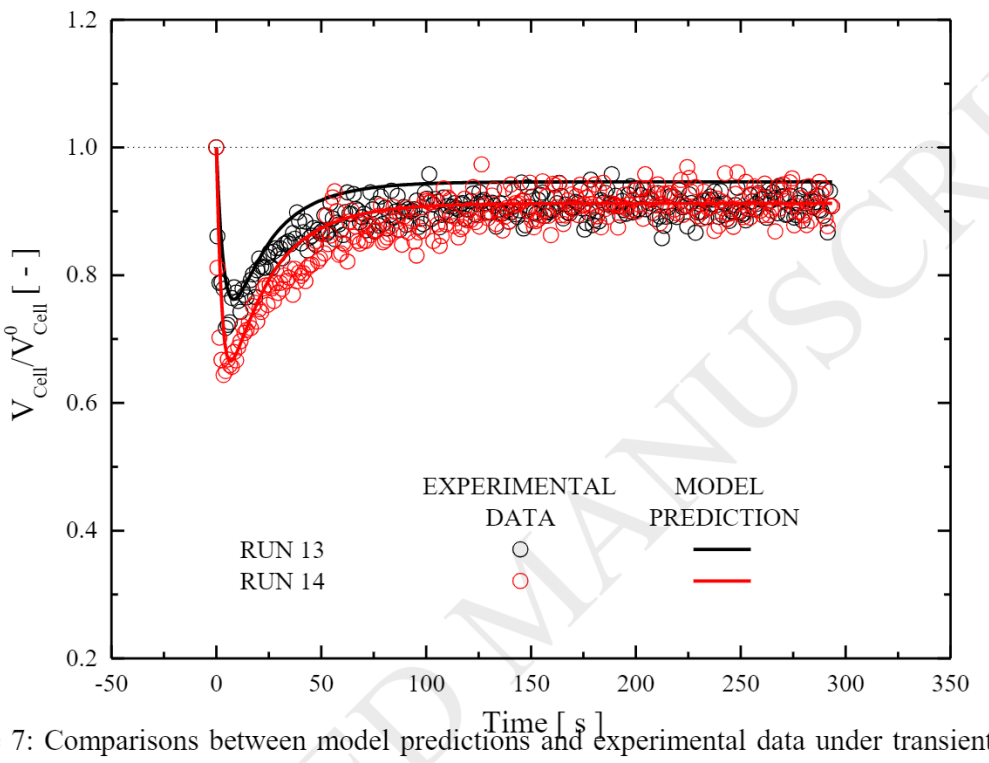

Figure 7: Comparisons between model predictions and experimental data under transient conditions for DMSO addition. Data measured by the authors [6].

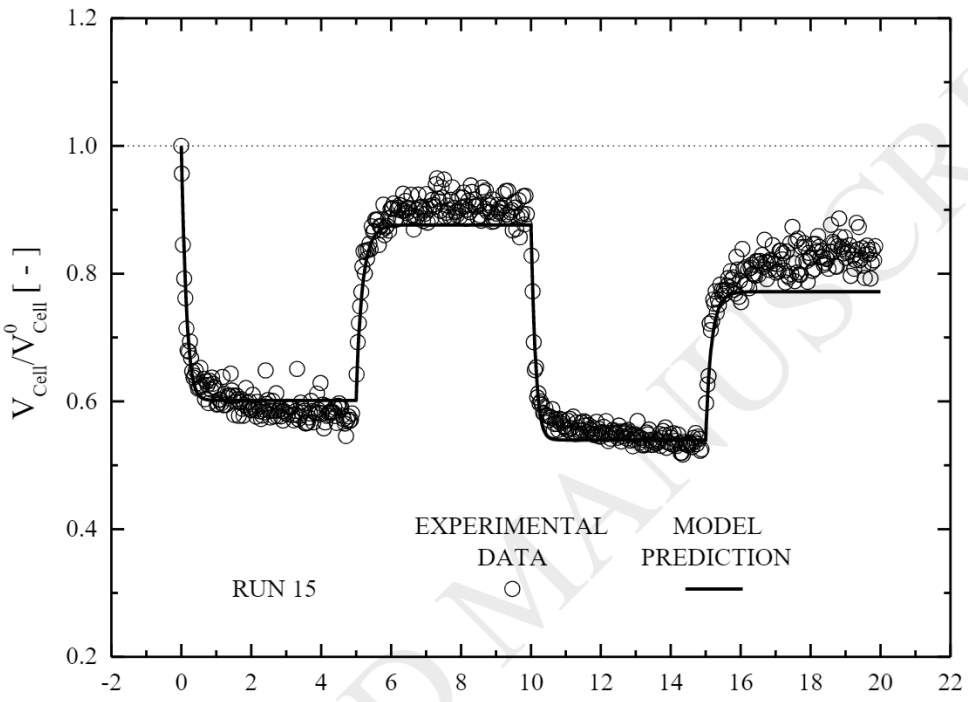

Figure 8: Comparisons between model predictions and experimental data under transient conditions for two consecutive osmotic cycles with sucrose. Data measured by the authors [7].

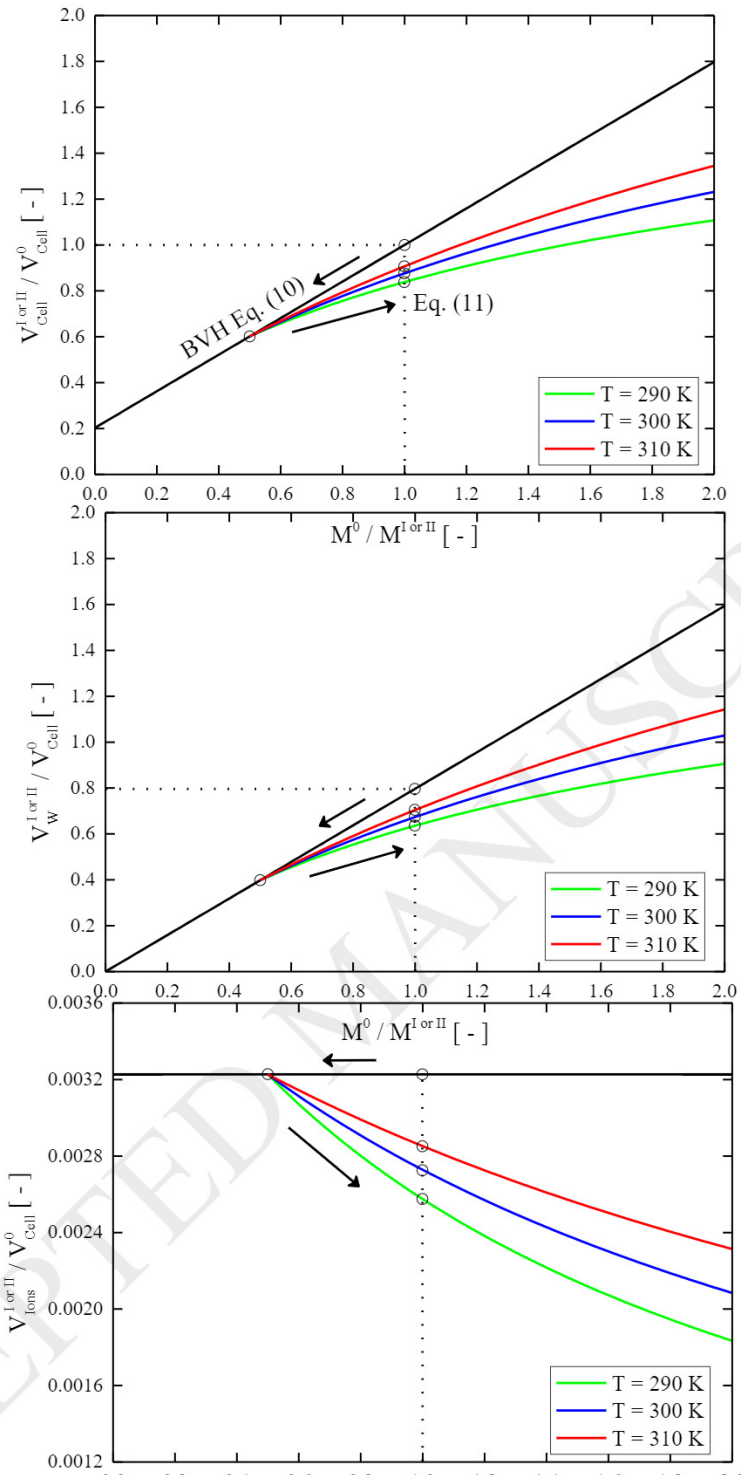

Figure 9: Equilibrium conditions for an osmotic cycle with impermeant sucrose: effect of temperature in terms of cell volume (a), with water (b) and ions (c) contributions. $M^0 = M_{\text{Ions}}^{\text{INT},0}$, $M^{\text{I}} = M^{\text{EXT, I}} = M_{\text{Ions}}^{\text{EXT,I}} + M_{\text{Sucrose}}^{\text{EXT,I}}$, $M^{\text{II}} = M^{\text{EXT, II}} = M_{\text{Ions}}^{\text{EXT,II}}$.

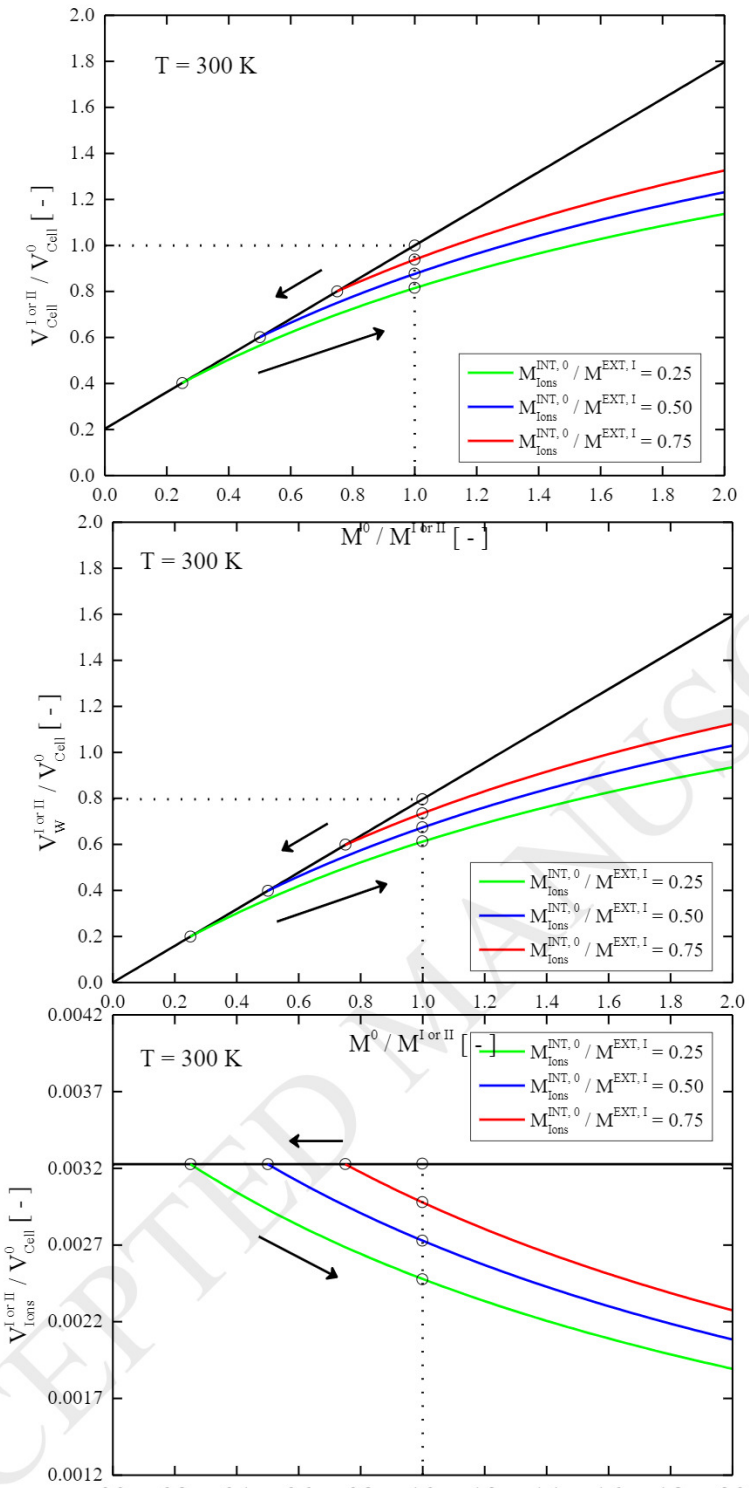

Figure 10: Equilibrium conditions for an osmotic cycle with impermeant sucrose: effect of external osmolality in terms of cell volume (a), with water (b) and ions (c) contributions. $M^{0} = M_{\mathrm{Ions}}^{\mathrm{INT},0}$, $M^{\mathrm{I}} = M^{\mathrm{EXT,\,I}} = M_{\mathrm{Ions}}^{\mathrm{EXT,I}} + M_{\mathrm{Sucrose}}^{\mathrm{EXT,I}}$, $M^{\mathrm{II}} = M^{\mathrm{EXT,\,II}} = M_{\mathrm{Ions}}^{\mathrm{EXT,II}}$.

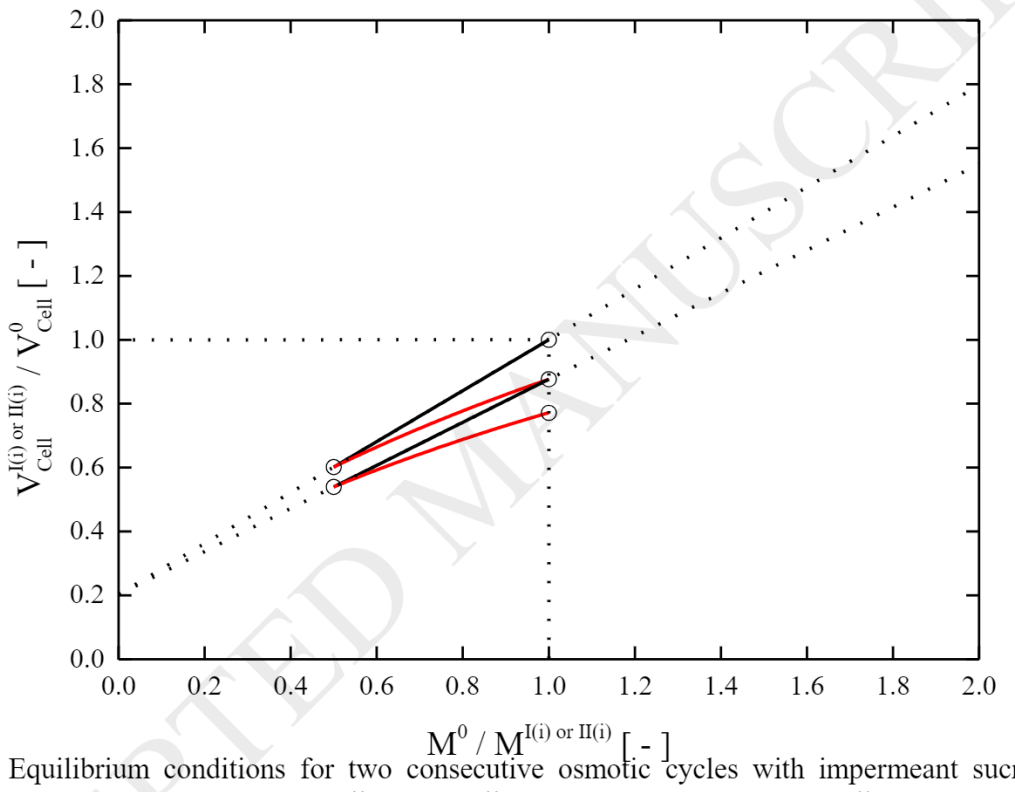

Figure 11: Equilibrium conditions for two consecutive osmotic cycles with impermeant sucrose. $M^{0} = M_{\text{Ions}}^{\text{INT},0}$, $M^{\text{I(i)}} = M^{\text{EXT, I(i)}} = M_{\text{Ions}}^{\text{EXT,I(i)}} + M_{\text{Sucrose}}^{\text{EXT,I(i)}}$, $M^{\text{II(i)}} = M^{\text{EXT, II(i)}} = M_{\text{Ions}}^{\text{EXT,II(i)}}$.